THE UNIVERSITY OF MICHIGAN
COLLEGE OF ENGINEERING
Department of Mechanical Engineering
Heat Transfer and Thermodynamics Laboratory

Progress Report No. 18

PRESSURIZATION OF LIQUID OXYGEN CONTAINERS

J. A. Clark
D. F. Jankowski
H. Merte, Jr.
W. O. Winer
V. S. Arpaci

UMRI Project 2646

under contract with:

DEPARTMENT OF THE ARMY
DETROIT ORDNANCE DISTRICT
CONTRACT NO. DA-20-018-ORD-15316
DETROIT, MICHIGAN

administered by:

THE UNIVERSITY OF MICHIGAN RESEARCH INSTITUTE ANN ARBOR

October 1959

ABSTRACT

The new experimental system has been put in operation. New instruments installed include a Minneapolis-Honeywell Visicorder Model 1012 to record thermocouple response, a liquid level indicator whose accuracy is within ± 1/16 of an inch of liquid level, and a recorder synchronizer. Experimental data have been obtained from this new system. Twenty-nine programmed runs have been made and the final mean density has been reduced from their records, both with and without external heat flux impressed by 120-v heaters. The inlet gas temperature is varied from -298°F to +107°F. These data are correlated with analytical work presented in Progress Reports 16 and 17.

An analytical study is reported on the time required to collapse a vapor bubble of nitrogen or oxygen in its liquid subsequent to pressurization.

The terminal rise velocities of vapor bubbles of nitrogen and oxygen has been investigated theoretically and results are given.

A new theoretical analysis of the response of the temperatures in the gas space and that of the container wall during pressurized-discharge has been started, and initial results are included. The analysis includes the influence of various ambient conditions and that of a container wall having finite thickness, and predicts both the gas and wall temperatures as functions or axial location and time.

NOMENCLATURE

A	Area, ft^2
A_o	Area, ft^2
b_1	See p. 12, hr^{-1}
b_2	See p. 12, hr^{-1}
b_3	See p. 12, hr^{-1}
b	$= b_2 + b_3$, hr^{-1}
c	Heat capacity of gas, $Btu/lb_m\text{-}F$
c^1	Heat capacity of wall, $Btu/lb_m\text{-}F$
Cp_L	Heat capacity of liquid, $Btu/lb_m\text{-}F$
C_D	Drag coefficient
g	Gravitational acceleration, ft/sec^2
g_c	Conversion factor, $lb_m\text{-}ft/lb_f\text{-}sec^2$
G_1	See Eq. (15)
h_{fg}	Latent heat, Btu/lb_m
h_g	Gas space heat-transfer coefficient, $Btu/hr\text{-}ft^2\text{-}F$
h_o	Ambinet heat-transfer coefficient, $Btu/hr\text{-}ft^2\text{-}F$
I_o	Bessel function of 1st kind, zeroth order
k_L	Thermal conductivity of liquid, $Btu/hr\text{-}ft\text{-}F$
m_v	Mass of vapor in bubble, lb_m
M	See Eq. (40)

NOMENCLATURE (Continued)

P_o	Perimeter, ft
P	Perimeter, ft
$q''(\theta)$	Time-dependent heat flux, Btu/hr-ft^2
q^*	See Eq. (30)
r	Radius, ft
r_1	Initial bubble radius, ft
Re	Reynolds number
R_b	Bubble radius, ft
S	See Eq. (29)
t	Temperature of liquid, F
t	Temperature of wall, F
t_1^*	Sat. temperature corresponding to p_1, F
t_2^*	Sat. temperature corresponding to p_2, F
T	Gas temperature, F
T_g	Step change in gas temperature, F
T_1, T_2	See p. 14
t_1, t_2	See p. 14
U	Terminal bubble velocity, ft/sec
V	Bubble volume, ft^3
V	Interfacial velocity, ft/sec
X	See p. 5

NOMENCLATURE (Concluded)

x	Axial coordinate, ft
Y	See p. 5
θ	Time, hr
θ_s	Bubble lifetime, hr
$\Phi(\theta)$	Arbitrary heat flux function
α_L	Thermal diffusivity of liquid $k_L/\rho_L Cp_L$, ft^2/hr
ρ	Density, lb_m/ft^3
μ	Viscosity, $lb_m/hr\text{-}ft$
η	See Eq. (31)
γ	Surface tension, lb_f/ft
ψ_2^{**}	See Eq. (33)
$\Lambda(\theta)$	See Eq. (42)
$\Pi(\theta)$	See Eq. (41)

A. EXPERIMENTAL PROGRAM

During the last period the new experimental system was completed and put into operation. Several programmed runs were made without external heat flux and with an external heat flux of approximately 1250 Btu/hr-ft^2. The inlet gas temperature for these runs varied from -298°F to 107°F. At present the results with inlet gas temperature between -298°F and -200°F are considered tentative because the thermocouple measuring the inlet gas temperature was influenced by condensed liquid from the inlet line which produced an indicated temperature which was variable. A new heat exchanger has been installed to correct this difficulty.

Twenty-nine runs have been made and reduced, of which 4 are tentative. Of the remaining 25, 13 are for no external heat flux with inlet temperature ranging from -125°F to +103°F. The 12 with heat flux consist of 6 with the heat flux imposed simultaneous with pressurization, 4 with the heat flux established about 5 minutes before pressurization, and 1 with heat flux on about 2 minutes before pressurization: The inlet gas temperature ranged from -80°F to 107°F for the heat flux runs. The final mean densities of all these runs are plotted in Fig. 1 as a function of inlet gas temperature. In this figure they are compared to the analytical work presented in Progress Reports 16 and 17. It is noted that, although the experimental results do not coincide with the theoretical analysis, they do follow the predicted shape.

In regard to the heat flux runs, the nominal value of heat flux (1250 Btu/hr-ft^2) was the value based on the power of the input to the heater circuit. This should not be taken for the heat flux into the liquid-gas system except during the period of preheat when the heaters are turned on for 5 minutes before pressurization. In this case, the system is at a steady-state boiling condition and the walls are at constant temperature. When the discharge begins in this type of run, and in all other runs made the energy into the heaters is partly retained in the walls, creating a temperature transient in the walls and the heater wires themselves; the remainder of the energy goes into the gas-liquid space.

From Fig. 1 it is noted that the value of heat flux used appears to have a very small—indeed, in some cases, an insignificant—effect on the final densities. The reason is that almost all the heat flux impressed in these cases goes into producing the temperature transient in the walls. A qualitative check of the temperature excersion in the walls during the discharge appears to bear this out.

Other work that has been done includes the calibration of the Minneapolis-Honeywell Model 1012 Visicorder. Each circuit and galvanometer was calibrated

individually and calibration curves relating the open circuit signal voltage and the deflection were made.

When the new Visicorder was introduced into the system, it was necessary to synchronize its timing system with that of the Sanborn and the Consolidated Oscillograph. The latter two were already synchronized. Synchronization of all three units was accomplished by connecting a coil, which has alternating current induced in it, and a switch in series with two parallel galvanometers circuits, one from the Visicorder and one from the Consolidated. When the switch is on, the alternating current is simultaneously recorded on both instruments and their timing systems are thereby synchronized.

The new heat exchanger which has just been installed is to facilitate obtaining steady inlet gas temperatures slightly above the saturation temperature of the nitrogen. With the present heat exchanger the low inlet gas temperatures were obtained by putting liquid nitrogen in the heat exchanger at atmospheric pressure, and consequently the gaseous nitrogen in the pipes at 50 psia condensed. This caused erratic behavior of the inlet gas temperature thermocouple and therefore produced unreliable data. The new heat exchanger is able to pressurize the liquid nitrogen coolant to pressures as high as 500 psi. When the coolant is pressurized, it will come to the new saturation temperature which can be made higher than the saturation temperature of the gas in the inlet pipes to the discharge container. In this way low inlet gas temperatures can be obtained but the gas will be superheated at constant temperature. The new heat exchanger was installed in parallel with the older one so either one can be used.

LIQUID LEVEL INDICATOR

The new design of the liquid level indicator has been completed and the instrument installed in the tank. Tests indicate that the uncertainty of this instrument in determining liquid level is better than ± 1/16 inch. The installation of a chromel wire as one of the contact wires proved to be very beneficial because the low temperature had a very corrosive effect on the copper wire. The corrosion of the copper wire caused unreliable contact resistance between the slide and the wire. The new design has the slide wipers mounted to a balsa wood float through a hinged arrangement. The wiper arrangement consists of two directly opposed copper slides mounted on arms which are both hinged about the same axis at the surface of the balsa wood float. This arrangement permits the wipers to remain directly opposed if the float should pitch and roll as it does during tank filling when the liquid boils violently, or if boiling should occur at any other time.

The main purpose of this instrument is to determine bubble volume by measuring the level drop of the boiling system upon pressurization. Preliminary tests show that this can be done readily. Figure 2 shows a recording of the pressurization and level drop. The voltage that is detected by the sliding

contacts is fed into the Sanborn recorder. The voltage across the wire is two volts, and the maximum attenuation on the Sanborn that can be used with this system is 0.002 volt per mm deflection which corresponds to 0.0355 in. of liquid level per millimeter of deflection on the Sanborn recording. With this attenuation and the zero suppression facilities of the Sanborn Recorder, there is a total deflection of 969 mm while the piston travels the length of the tank.

It is noted from Fig. 2 that the level indicator has the ability to detect not only the level drop upon pressurization but also the excessive rise in level when the pressure is released from the liquid. Upon depressurization the liquid is superheated and violently flashes momentarily into a boiling state.

Since these data have been taken, new quick-acting valves have been installed so that the system can be more rapidly pressurized and depressurized.

Figure 3 shows the record of the level indicator during the discharge of a normal run to demonstrate the smooth behavior of the instrument.

WORK DURING THE NEXT PERIOD

During the next period programmed runs will be made employing the new heat exchanger to provide a wider range of inlet temperature data. When this has been completed, the range of inlet gas temperature will be run again using the heat flux produced by 220 v on the heater circuits. This will provide a maximum heat flux of about 5000 Btu/hr-ft^2. The possibility of also using 440 v will be investigated. A system incorporating an insulating material on the inside surface of the container will be assembled which will provide results giving a broader understanding of the mechanisms of pressurized discharge processes.

B. COLLAPSE OF OXYGEN AND NITROGEN VAPOR BUBBLES IN THEIR LIQUIDS FOLLOWING A SUDDEN PRESSURIZATION

A theoretical study has been completed on the collapse of vapor bubbles of oxygen and nitrogen in their liquids following a sudden pressurization. This condition exists when an initially boiling liquid is suddenly pressurized. The vapor in the bubbles and the liquid are initially at the saturation temperature corresponding to the initial pressure. Subsequent to pressurization, however, the vapor obtains a saturation condition which has a corresponding temperature equal to the saturation temperature at the pressurizing pressure. The liquid remains at its initial saturation temperature in the regions well removed from the liquid-vapor interface. As a consequence of the pressurization, vapor at the higher saturation temperature condenses on the vapor-liquid interface, increasing and maintaining the temperature there until the bubble has completely condensed. For purposes of analysis it will

be assumed that this process causes a sudden increase in the temperature of this interface from the saturation temperature corresponding to the initial pressure to that of the final pressure. Also indicant of the pressurization is a reduction in volume of the bubbles owing to the vapor-density change resulting from the increased pressure. This will be assumed to occur instantaneously to the density of a saturated vapor at the final pressure. The analysis ignores the displacement of the interface. Such movement would tend to increase the condensation rates and shorten the bubble life times as herein computed.

The transient temperature distribution around a spherical cavity of radius r_1 in an infinite expanse of liquid resulting from a sudden increase in temperature at the liquid-vapor interface may be found from an analysis of Crank,[1] as

$$\frac{t(r,\theta) - t_2^*}{t_1^* - t_2^*} = \frac{r_1}{r} \operatorname{erfc} \frac{r-r_1}{2\sqrt{\alpha_L \theta}} = \frac{r_1}{r}\left[1 - \operatorname{erf} \frac{r-r_1}{2\sqrt{\alpha_L \theta}}\right] \tag{1}$$

The radial gradient in temperature in the liquid at the interface is found through differentiation of Eq. (1) to be

$$-\left(\frac{\partial t}{\partial r}\right)_{r_1} = (t_1^* - t_2^*)\left[\frac{1}{r_1} + \frac{1}{\sqrt{\pi \alpha_L \theta}}\right] \tag{2}$$

Now, the amount of heat transferred through this interface in time θ resulting from condensation of vapor there is written

$$Q = m_v h_{fg} = \int_0^{\theta} - k_L (4\pi r_1^2) \left(\frac{\partial t}{\partial r}\right)_{r_1} d\theta \tag{3}$$

To condense all the vapor mass initially within a bubble of radius r_1, Eq. (3) becomes

$$\frac{4}{3}\pi r_1^3 \rho_l h_{fg} = 4\pi r_1^2 k_L (t_1^* - t_2^*) \int_0^{\theta_s} \left[\frac{1}{r_1} + \frac{1}{\sqrt{\pi \alpha_L \theta}}\right] d\theta \tag{4}$$

Upon integration and rearrangement, Eq. (4) is written

$$\frac{\rho_l}{\rho_L C_{p_L}} \frac{h_{fg}}{t_1^* - t_2^*} = \frac{\sqrt{\pi \alpha_L \theta_s}}{r_1}\left[\frac{\sqrt{\pi \alpha_L \theta_s}}{r_1} + 2\right]\frac{3}{\pi} \tag{5}$$

or

$$Y = X[X+2]\frac{3}{\pi} \tag{6}$$

where

$$X = \frac{\sqrt{\pi \alpha_L \theta_s}}{r_1} , \qquad Y = \frac{\rho_1}{\rho_L \, Cp_L} \cdot \frac{h_{fg}}{t_1^* - t_2^*}$$

Equation (6) is a generalized result in dimensionless form which may be used to compute the lifetime θ_s of a vapor bubble initially of radius r_1 in terms of the properties of the liquid and vapor and the increase in temperature at the bubble interface. Equation (6) is plotted in Fig. 4.

It will be observed that X is a singled-valued function of Y, the function passing through the point X = 0, Y = 0. For a fixed value of X the bubble lifetime θ_s is proportional to

$$\theta_s \sim \frac{r_1^2}{k_L/\rho_L Cp_L} \tag{7}$$

Hence, small lifetimes are associated with small initial bubbles and liquids of large thermal diffusivity, $k_L/\rho_L Cp_L$. Also small values of X correspond to systems having large temperature differences imposed on the liquid-vapor interface.* This is equivalent to having large pressure increases imposed.

In the case of liquid nitrogen pressurized from 15 psia to 50 psia, the value of Y is 0.126. This gives a value of X of about 0.05. Hence

$$\theta_s = (0.05)^2 \frac{r_1^2}{\pi \alpha_L} = \frac{(25)10^{-4}}{(53.5)10^{-4}} \cdot \frac{r_1^2}{\pi}$$

$$= 0.149 \, r_1^2$$

For a bubble having a radius of 0.02 ft (approximately 1/2-in. diam) the bubble lifetime is about 0.215 sec. Should the bubble be one-half that size, or 1/4-in. diam, its lifetime would be 1/4 as great, or about 0.054 sec.

Bubbles of oxygen vapor in liquid oxygen may be expected to behave in a similar way owing to the similarity in its properties with nitrogen.

C. A STUDY OF THE RISE VELOCITIES OF VAPOR BUBBLES IN LIQUID NITROGEN AND LIQUID OXYGEN

The motion of a vapor bubble in a liquid of infinite expanse is described in terms of a drag coefficient, C_D. The drag coefficient in turn is a function of the Reynolds number, Re, of the bubble based on the properties of the

*This dependence can be seen from Eq. (6) or Fig. 4.

liquid. The relation between C_D and Re depends to a certain extent on the type of liquid.

Observations and descriptions of rising bubbles in liquids under the action of normal gravitational buoyancy have been made by many investigators. For the purpose of this study, the results of Peebles and Garber[2] and Haberman and Morton[3] have been used as representative. Drag coefficient data taken from these two sources have been related to liquid nitrogen (as described below) and the result is given in Fig. 5 as a function of the Reynolds number of the bubble. Similar data have been computed for liquid oxygen which give essentially the same results. As is noted, considerable difference is found between curves A-A and B-B of Fig. 5. However, the data of Peebles and Garber have been corrected to the conditions of saturated liquid nitrogen at a pressure of one atmosphere while those of Haberman and Morton have not. This is partly the reason for the difference between the two results.

Four regimes of flow are used to describe the bubble motion. For conditions of saturated liquid nitrogen and oxygen at one atmosphere, these are approximately as follows:

(a) Rigid sphere. For Re less than 2. Bubbles are spherical and move in rectilinear paths. C_D agrees with results predicted by Stokes' Law.

(b) Fluid sphere. For Re greater than 2 and less than about 936 for liquid nitrogen and 1175 for liquid oxygen (see below for discussion of this limit). Bubbles are roughly spherical and some slip is expected to exist at vapor-liquid boundary. Movement is in rectilinear paths. C_D is somewhat less than that predicted from Stokes' Law.

(c) Re greater than 936 or 1175 and less than 1790 or 2090 for liquid nitrogen and liquid oxygen, respectively. Bubbles deformed to ellipsoidal cross section and flattened horizontally. Interfacial condition unknown. Probably of the nature of a fluid sphere with significant wake influence. Motion in spiraling, zig-zag paths. C_D increases sharply with Re.

(d) Bubbles greatly deformed with hemi-spherical caps. Both interfacial slip and wake probably important. Re greater than 1790 or 2090. Bubble motion in rectilineal path. Bubble velocity appears to be independent of liquid properties. Disagreement exists as to whether C_D increases with Re or remains constant in this range. Evidence[3] appears to support the latter. Data of Peebles and Garber[2] in this range are possibly influenced by walls of container.

Data from both Refs. 2 and 3 are used in the computations reported here. Those of Peebles and Garber[2] have been corrected for temperature and pressure

while those of Haberman and Morton[3] have not. This resulted from the fact that criteria for such a correction were given in Ref. 2 but not in Ref. 3. However, the consequence is an upper and a lower limit to the bubble velocities which might reasonably be expected.

The velocity-diameter results are given in Fig. 6 for liquid nitrogen and Fig. 7 for liquid oxygen. The results are practically identical but are shown on two curves to avoid confusion. Above a diameter of about 0.100 in., two velocity curves are given in each figure.

The results for curves A-A are thought to be unrealistic and it is expected they should follow curves B-B more closely in this region. This is the region of flow regime of type (d) in which Peebles and Garber found an increasing C_D with Re, contrary to that found by Haberman and Morton whose results indicated a constant value of C_D in this range of Re. It is important to note that the experiments of Peebles and Garber extended only to an Re of about 3000 while those of Haberman and Morton were conducted at an Re of up to 10,000. Hence it seems that the measurements of Haberman and Morton more completely describes the bubble motion at high Reynolds numbers, flow regime (d). It seems possible that the results of Peebles and Garber were not carried to sufficiently high values of the Reynolds number and that the bubbles at their maximum Re were not actually in regime (d) but in a transition region between regime (c) and (d). Another important point is that any influence of the container walls is much more likely to show up in the experiment of Peebles and Garber than in those of Haberman and Morton. Peebles and Garber used a 1.03-in.-ID tube and report a definite influence of the container walls on the motion of large bubbles. Haberman and Morton used a minimum sized test section of 6 by 6 inches in cross section, and found no influence of any effects of the wall on the larger bubbles. It is for this reason that more confidence is placed in the results of Haberman and Morton in the range of large bubbles for calculations of bubble velocities in liquids of infinite expanse.

CALCULATION PROCEDURE

When a bubble moves through a liquid at its terminal velocity, the net drag force acting on the surface of the bubble is balanced by the net buoyant force. Hence

$$C_D A \frac{\rho_1 U^2}{2g_c} = V \frac{g}{g_c} (\rho_1 - \rho_2) \tag{8}$$

For equivalent spherical bubbles $A = \pi R_b^2$ and $V = 4/3\ \pi R_b^3$. Equation (8) rearranged becomes:

$$C_D U^2 = \frac{4}{3} g \left(1 - \frac{\rho_2}{\rho_1}\right) 2R_b \tag{9}$$

The Reynolds number of the bubble is defined as

$$Re \equiv \frac{(2R_b)U\rho_1}{\mu_1} \tag{10}$$

or

$$2R_b = \frac{Re}{R_b}\left(\frac{\mu_1}{\rho_1}\right) \tag{11}$$

Substituting Eq. (11) into Eq. (9) and rearranging gives

$$U = \left[\left(\frac{Re}{C_D}\right)\frac{\mu_1}{\rho_1}\left(1 - \frac{\rho_2}{\rho_1}\right)\frac{4}{3}g\right]^{1/3} \tag{12}$$

And, from Eq. (11),

$$R_b = \frac{Re\ (\mu_1/\rho_1)}{2U} \tag{13}$$

Further, from experimental correlations such as those in Refs. 2 and 3 corrected or uncorrected for temperature and pressure, one has

$$C_D = f(Re) \tag{14}$$

The key to the entire calculation is the selection of the relation between C_D and Re, Eq. (14). The two such relationships taken for this study are shown in Fig. 5. It is felt that up to a Reynolds number of about 1000 this is the more realistic relationship. It also predicts results which probably are conservative, i.e., higher bubble velocities than are anticipated. However, it must be emphasized that the original data of Ref. 2 was for room-temperature water and considerable extrapolation is required to extend the data to the conditions of saturated liquid oxygen and nitrogen at a pressure of one atmosphere. Furthermore, the basic process is not well understood, especially at the point of transition corresponding to the maximum bubble velocity. Curve B is taken from Haberman and Morton,[3] whose results probably predict the velocity of the larger bubbles more realistically than that of the smaller bubbles.

The method of calculation is to fix the Re and compute a value of C_D from Eq. (14). Then the value of the bubble velocity, U, is found from Eq. (12). The corresponding equivalent bubble radius, R_b, is calculated from Eq. (13). This process is repeated throughout the range of Re from 1 to 10,000.

The resulting bubble velocity curves are given in Figs. 6 and 7 as U in ft/sec vs. D_b in inches.

CALCULATIONS

Peebles and Garber[2] recommend a relationship between C_D and Re for each of the four flow regimes discussed earlier. They also give criteria for the transition from one regime to another. This transition is probably not sharp as shown on Fig. 5, but for the purposes of this calculation it will be assumed as such. The following relationships are used.

Flow Regime	$C_D = f(Re)$	Limits
(a)	$C_D = 24/Re$	$Re \leq 2$
(b)	$C_D = 18.7/Re^{0.68}$	$2 \leq Re \leq 4.02/G_1^{0.214}$
(c)	$C_D = 0.0275\ G_1\ Re^4$	$4.02/G_1^{0.214} \leq Re \leq 3.10/G_1^{0.250}$
(d)	$C_D = 0.82\ G_1^{0.25}\ Re$	$Re \leq 3.10/G_1^{0.250}$

In this set of criteria G_1 is defined as

$$G_1 = \frac{g\mu_1^4}{\rho_1 \gamma_1^3 g_c^3} \tag{15}$$

Re Limits for Calculations

Flow Regime	Liquid Nitrogen	Liquid Oxygen
(a)	$Re \leq 2$	$Re \leq 2$
(b)	$2 \leq Re \leq 936$	$2 \leq Re \leq 1175$
(c)	$936 \leq Re \leq 1790$	$1175 \leq Re \leq 2090$
(d)	$Re \leq 1790$	$Re \leq 2090$

This calculation of these limits is subject to some approximation for two reasons. First, the validity of it as a criterion for transition is not well established; and, second, the numerical value of the critical Reynolds numbers is dependent on γ^3, which greatly magnifies any influence of uncertainties in γ. The numerical values of γ used in these calculations were 0.906×10^{-3} lb_f/ft for liquid oxygen and 0.606×10^{-3} lb_f/ft for liquid nitrogen and were obtained through a private communication.

The calculation procedure was as outlined above. The numerical results are tabulated below for liquid nitrogen and liquid oxygen.

Re	C_D	U ft/in.	U ft/sec	$R_b \times 10^3$ ft	$R_b \times 10^3$ in.	$D_b \times 10^3$ in.
			Liquid Nitrogen			
1	24	54.7	0.0152	0.0658	0.790	1.580
2	12	86.9	0.0241	0.0830	0.996	1.992
5	6.27	146.5	0.0407	0.1228	1.472	2.944
10	3.91	216.0	0.0600	0.1667	2.000	4.000
50	1.31	532.5	0.148	0.338	4.06	8.12
100	0.816	784.5	0.218	0.459	5.50	11.00
300	0.386	1452	0.403	0.745	8.94	17.88
500	0.274	1930	0.536	0.934	11.20	22.40
800	0.199	2510	0.698	1.145	13.75	27.50
936	0.178	2750	0.765	1.222	14.69	29.38
1,100	0.258	2560	0.710	1.550	18.60	37.20
1,400	0.936	1806	0.502	2.79	33.50	67.00
1,700	2.04	1485	0.412	4.13	49.60	99.20
1,790	2.51	1412	0.393	4.55	54.60	109.20
2,000	2.60	1448	0.402	4.97	59.60	119.20
3,000	2.60	1657	0.460	6.53	78.40	156.80
5,000	2.60	1962	0.545	9.19	110.2	220.4
7,000	2.60	2200	0.611	11.45	137.4	274.8
10,000	2.60	2480	0.689	14.51	174.2	348.4
			Liquid Oxygen			
1	24	52.9	0.0147	0.0610	0.731	1.462
2	12	83.95	0.0233	0.0770	0.924	1.848
5	6.27	141.5	0.0393	0.1142	1.37	2.74
10	3.91	208.5	0.0580	0.1543	1.85	3.70
50	1.31	515	0.1430	0.3134	3.76	7.52
100	0.816	760	0.2110	0.4250	5.10	10.20
300	0.386	1400	0.389	0.691	8.29	16.58
500	0.274	1860	0.516	0.869	10.42	20.84
1,000	0.171	2750	0.764	1.172	14.10	28.20
1,175	0.254	2540	0.705	1.496	17.90	35.80
1,500	0.675	1990	0.553	2.430	29.15	58.30
2,000	2.13	1495	0.416	4.310	51.6	103.2
2,090	2.54	1430	0.398	4.71	56.5	113.0
2,500	2.60	1506	0.419	5.35	64.1	128.2
3,000	2.60	1600	0.445	6.05	72.6	145.2
5,000	2.60	1898	0.527	8.51	102.0	204.0
7,000	2.60	2120	0.589	10.68	128.0	256.0
10,000	2.60	2390	0.665	13.5	162.0	324.0

D. ANALYSIS OF GAS- AND WALL-TEMPERATURE RESPONSE DURING THE DISCHARGE OF A CRYOGENIC LIQUID FROM A CONTAINER

In Progress Report 15 an analysis was presented of the response of the gas temperature during the process of discharge of a liquid from a closed container. This type of analysis is extended in this report using a somewhat more refined theoretical model. In the previous work it was necessary for purposes of heat-transfer analysis to ignore the influence of an ambient and to assume that the gas temperature was constant and that the container wall was of infinite thickness. All these limitations are removed in the present analysis which treats heat exchange with the following three types of ambient conditions through a container wall of finite thickness:

(a) Container insulated from ambient.
(b) Container exchanging heat with an ambient of constant temperature.
(c) Container exchanging heat with an ambient by means of an arbitrarily time dependent heat flux.

The analytical model is shown in Fig. 8. For this analysis the following assumptions are made.

(a) Gas and wall temperatures refer to the radial mean values and are functions of axial distance and time.
(b) The gas-liquid interface is flat and moves at a constant velocity with respect to the wall.
(c) The influence of axial heat conduction in both gas and wall is negligible.
(d) The gas and the ambient exchange heat with the walls through coefficients of heat transfer which are constant. All physical properties of gas and liquid are constant.
(e) Heat transfer from the gas is with the container walls only. It was shown in Progress Report 17 that the wall-gas heat transfer is the more significant transfer. Heat transfer with the container top and with the liquid interface will be investigated later as a superimposed effect.
(f) The transients are introduced by a step-change in the gas inlet temperature and/or by an arbitrary time dependent heat flux on the outer surface of the container.
(g) Initially the gas and wall have the same temperature which may be taken equal to zero.

Within these assumptions the first law of thermodynamics applied to the gas and the wall produces the following partial differential equations.

Case I Heat Transfer with the Ambient

Gas:

$$\frac{\partial T}{\partial \theta} + V \frac{\partial T}{\partial x} + b_1(T-t) = 0 \tag{16}$$

Wall:

$$\frac{\partial t}{\partial \theta} - b_2(T-t) + b_3 t = 0 \tag{17}$$

with the following boundary conditions:

$$T(x,0) = 0 \tag{18}$$

$$t(x,0) = 0 \tag{19}$$

$$T(0,\theta) = T_g \tag{20}$$

Case II Time-Dependent Heat Flux from the Ambient

Gas:

$$\frac{\partial T}{\partial \theta} + V \frac{\partial T}{\partial x} + b_1(T-t) = 0 \tag{21}$$

Wall:

$$\frac{\partial t}{\partial \theta} - b_2(T-t) - \Phi(\theta) = 0 \tag{22}$$

with the same boundary conditions, Eqs. (18), (19), and (20) applied. In Eqs. (16) - (22) the following quantities are defined:

$$b_1 = \frac{h_g P}{\rho C A}$$

$$b_2 = \frac{h_g P}{\rho' C' A_o}$$

$$b_3 = \frac{h_o P_o}{\rho' C' A_o}$$

$$\Phi(\theta) = \frac{q''(\theta) P_o}{\rho' C' A_o}$$

$$\theta = \text{Time}$$

Case III Container Insulated from Ambient

This is a special case of Case I in which b_3 is equal to zero. Hence

Gas:

$$\frac{\partial T}{\partial \theta} + V \frac{\partial T}{\partial x} + b_1(T-t) = 0 \tag{23}$$

Wall:

$$\frac{\partial t}{\partial \theta} - b_2(T-t) = 0 \tag{24}$$

Equations (16) and (17) are operated on by the Laplace transform technique, the transformed equations integrated with the appropriate boundary conditions, and inverse transformation performed. The results are

$0 \leq V\theta/x \leq 1$

$$T(x,\theta) = 0 \tag{25}$$

$$t(x,0) = 0 \tag{26}$$

$V\theta/x \geq 1$

$$T/T_g = e^{-S} \left\{ \psi_2^{**}(\eta S, q^*) + e^{-q^*} I_0[2(\eta S q^*)^{1/2}] \right\} \tag{27}$$

$$t/T_g = \eta\, e^{-S}\, \psi_2^{**}(\eta S, q^*) \tag{28}$$

where

$$S = \frac{b_1 x}{V} \tag{29}$$

$$q^* = b\,(\theta - x/V) \tag{30}$$

$$\eta = \frac{b_2}{b_2 + b_3} \tag{31}$$

$$b = b_2 + b_3 \tag{32}$$

$$\psi_2^{**}(\eta S, q^*) = \sum_{k=0}^{\infty} \frac{(\eta S)^k}{(k!)^2} \int_0^{q^*} z^k e^{-z}\, dz \tag{33}$$

$I_0(\ )$ = Bessel function of first kind, zero order

A similar problem has been previously solved for an insulated container.[8] The above equations for $\eta=1$, which corresponds to $b_3 = 0$, give the solution for Case III, in which the container is insulated from the ambient. The tabulation of ψ_2** may be found in two other papers[4,5] and is reproduced here from Ref. 5 in Fig. 9. In this figure the parameter (S) is to be interpreted as (ηS) of Eqs. (29), (31), and (33) and the parameter (q) is to be interpreted as (q*) of Eq. (30).

The second problem, Case II, for a time-dependent heat flux from the ambient, is solved using the principle of superposition of solutions. That is, the functions T and t can be divided into the two following functions:

$$T = T_1 + T_2 \tag{34}$$

and

$$t = t_1 + t_2 \tag{35}$$

where the pair T_1,t_1 results from a step temperature change in the gas temperature with no heat transfer at the outer surface. As indicated, this solution corresponds to Case III, which is Eqs. (27) and (28) for $\eta = 1$. The other pair, T_2,t_2, results from a time-dependent heat flux at the outer surface with no change in the gas temperature. The governing differential equation has been solved previously in connection with another study.[5-7] The solutions may be summarized as follows.

<u>$0 \leq V\theta/x \leq 1$</u>

$$t_2(\theta) = \frac{M}{M+1} \int_0^\theta \Phi(S) \left[1 + \frac{1}{M} e^{\frac{b_1(M+1)}{M}(S-\theta)}\right] ds \tag{36}$$

$$\Delta T_2(\theta) = e^{-\frac{b_1(M+1)}{M}\theta} \int_0^\theta \Phi(S)\, e^{\frac{b_1(M+1)}{M}S}\, ds \tag{37}$$

<u>$V\theta/x \geq 1$</u>

$$t_2(x,\theta) = \frac{M}{M+1}\left\{\int_0^\theta \Phi(S)\left[1 + \frac{1}{M} e^{\frac{b_1(M+1)}{M}(S-\theta)}\right] ds - \frac{b_1}{M} e^{-\frac{b_1 x}{V}} \int_0^{\theta^*} \Pi(\theta-S)\, e^{-\frac{b_1}{M}S}\, I_0\left[2b_1\left(\frac{Sx}{MV}\right)^{1/2}\right] ds\right\} \tag{38}$$

$$\Delta T_2(x,\theta) = e^{\frac{b_1(M+1)}{M}\theta} \int_0^\theta \Phi(S)\, e^{-\frac{b_1(M+1)}{M}S}\, ds + b_1 e^{-\frac{b_1 x}{V}} \int_0^{\theta^*} \Lambda(\theta-S)\, e^{-\frac{b_1 S}{M}}\, I_0\left[2b_1\left(\frac{Sx}{MV}\right)^{1/2}\right] ds \tag{39}$$

where

$$M = \frac{b_2}{b_1} \tag{40}$$

$$\Pi(\theta) = \int_0^\theta \Phi(z)dz - \Lambda(\theta) \tag{41}$$

$$\Lambda(\theta) = e^{-\frac{b_1(M+1)}{M}\theta} \int_0^\theta \Phi(z)\, e^{\frac{b_1(M+1)}{M}S}\, ds \tag{42}$$

$$\Delta T_2(\theta) = t_2(\theta) - T_2(\theta) \tag{43}$$

$$\Delta T_2(x,\theta) = t_2(x,\theta) - T_2(x,\theta) \tag{44}$$

During the next period these theoretical results will be evaluated and a comparison made with existing experimental data. In addition the influence of the top of the container and that of the liquid-vapor interface will be investigated.

REFERENCES

1. Crank, J., Mathematics of Diffusion, Oxford Press, 1956, p. 98.

2. Peebles, F. N., and Garber, H. J., "Studies on the Motion of Gas Bubbles in Liquids," Chemical Engineering Progress, 49, 88 (February, 1953).

3. Haberman, W. L., and Morton, R. K., "An Experimental Study of Bubbles Moving in Liquids," Proceedings, American Society of Civil Engineers, 80, Separate No. 387, January, 1954.

4. Rizika, J. W., "Thermal Lags in Flowing Incompressible Fluid Systems Containing Heat Capacitors," Trans. ASME, 78, 1407 (1956).

5. Clark, J. A., Arpaci, V. S., and Treadwell, K. M., "Dynamic Response of Heat Exchangers Having Internal Heat Sources - Part I," Trans. ASME, 80, 612-624 (1958).

6. Arpaci, V. S., and Clark, J. A., "Dynamic Response of Heat Exchangers Having Internal Heat Sources - Part II," Trans. ASME, 80, 625-634 (1958).

7. Arpaci, V. S., and Clark, J. A., "Dynamic Response of Heat Exchangers Having Internal Heat Sources - Part III," to be published Journal of Heat Transfer, ASME, December, 1959.

8. Carslaw, H. S., and Jaeger, J. C., Conduction of Heat in Solids, Oxford Univ. Press, London, 1948, pp. 326-328.

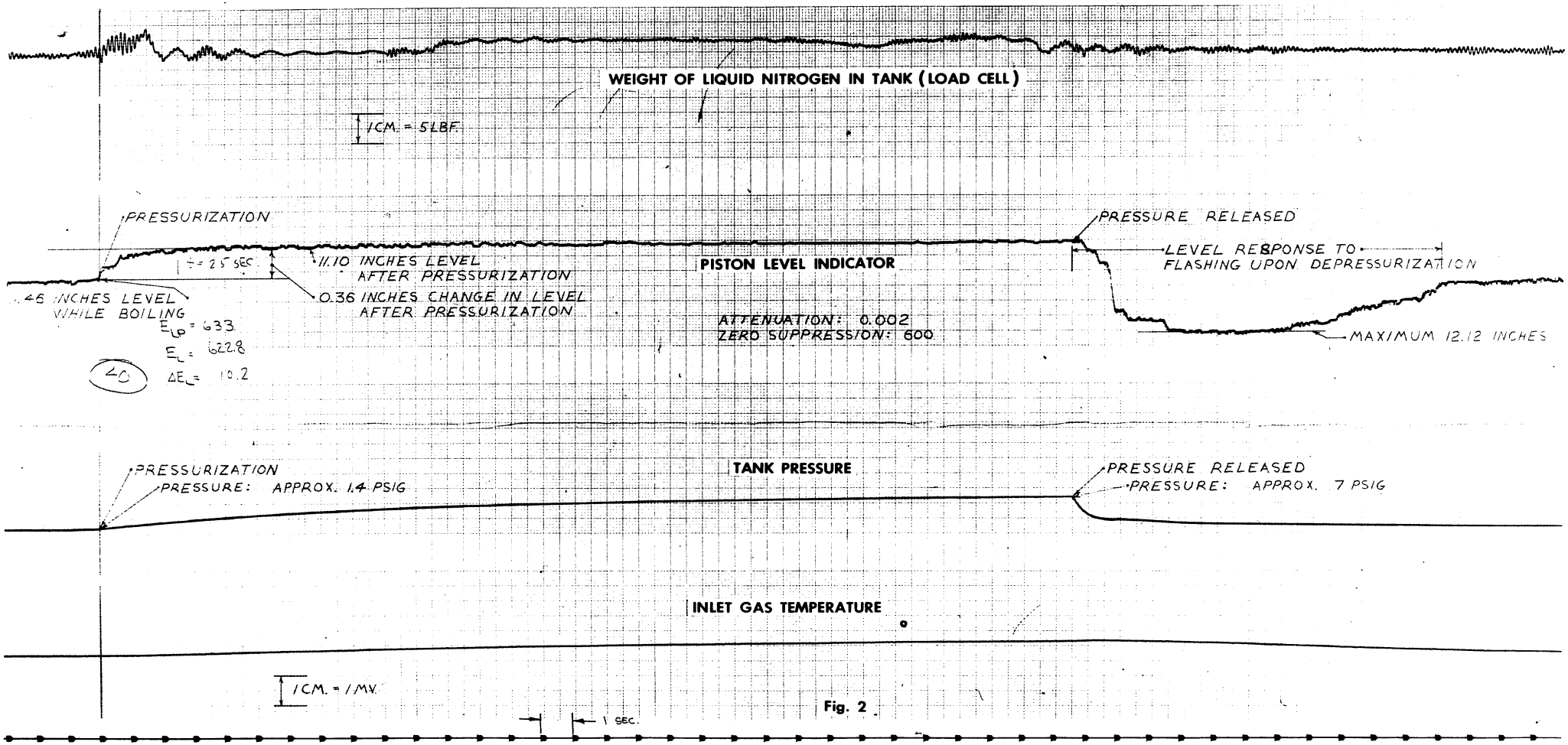
WEIGHT OF LIQUID NITROGEN IN TANK (LOAD CELL)
1 CM. = 5 LBF.
PRESSURIZATION
PRESSURE RELEASED
1 = 2.5 SEC.
11.10 INCHES LEVEL
AFTER PRESSURIZATION
.46 INCHES LEVEL
WHILE BOILING
0.36 INCHES CHANGE IN LEVEL
AFTER PRESSURIZATION
PISTON LEVEL INDICATOR
LEVEL RESPONSE TO
FLASHING UPON DEPRESSURIZATION
ATTENUATION: 0.002
ZERO SUPPRESSION: 600
MAXIMUM 12.12 INCHES
E_{LP} = 633
E_L = 622.8
40
ΔE_L = 10.2
PRESSURIZATION
PRESSURE: APPROX. 1.4 PSIG
TANK PRESSURE
PRESSURE RELEASED
PRESSURE: APPROX. 7 PSIG
INLET GAS TEMPERATURE
1 CM. = 1 MV.
1 SEC.

Fig. 2

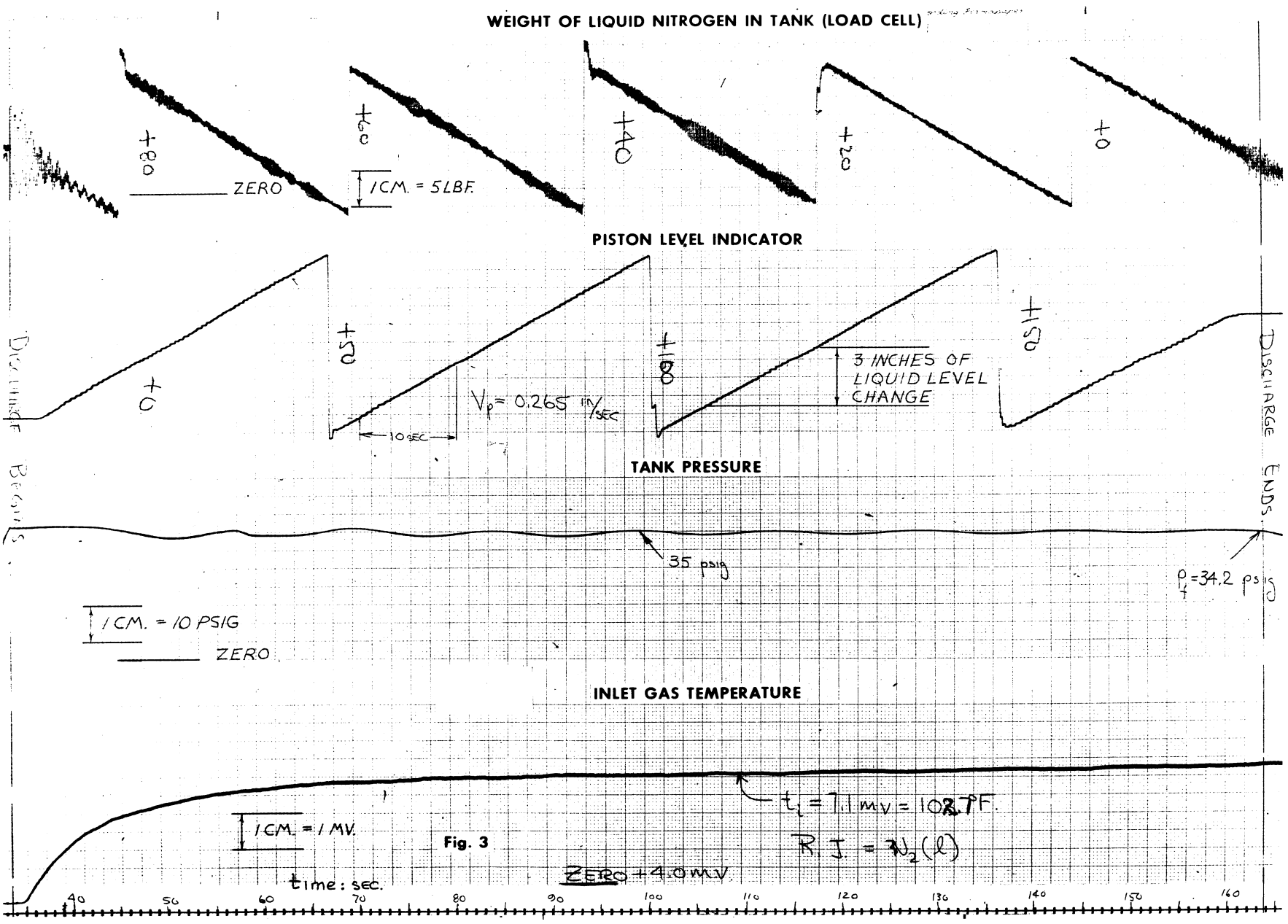
WEIGHT OF LIQUID NITROGEN IN TANK (LOAD CELL)
+80
ZERO
+60
1 CM. = 5 LBF.
+40
+20
+0
PISTON LEVEL INDICATOR
+0
+25
+10
+15
V_p = 0.265 IN/SEC
10 SEC
3 INCHES OF LIQUID LEVEL CHANGE
DISCHARGE BEGINS
DISCHARGE ENDS
TANK PRESSURE
35 psig
P_f = 34.2 psig
1 CM. = 10 PSIG
ZERO
INLET GAS TEMPERATURE
t_i = 7.1 mV = 102°F.
$R_T = R_2(l)$
1 CM. = 1 MV.
ZERO + 4.0 mV
time: sec.
40
50
60
70
80
90
100
110
120
130
140
150
160

Fig. 3

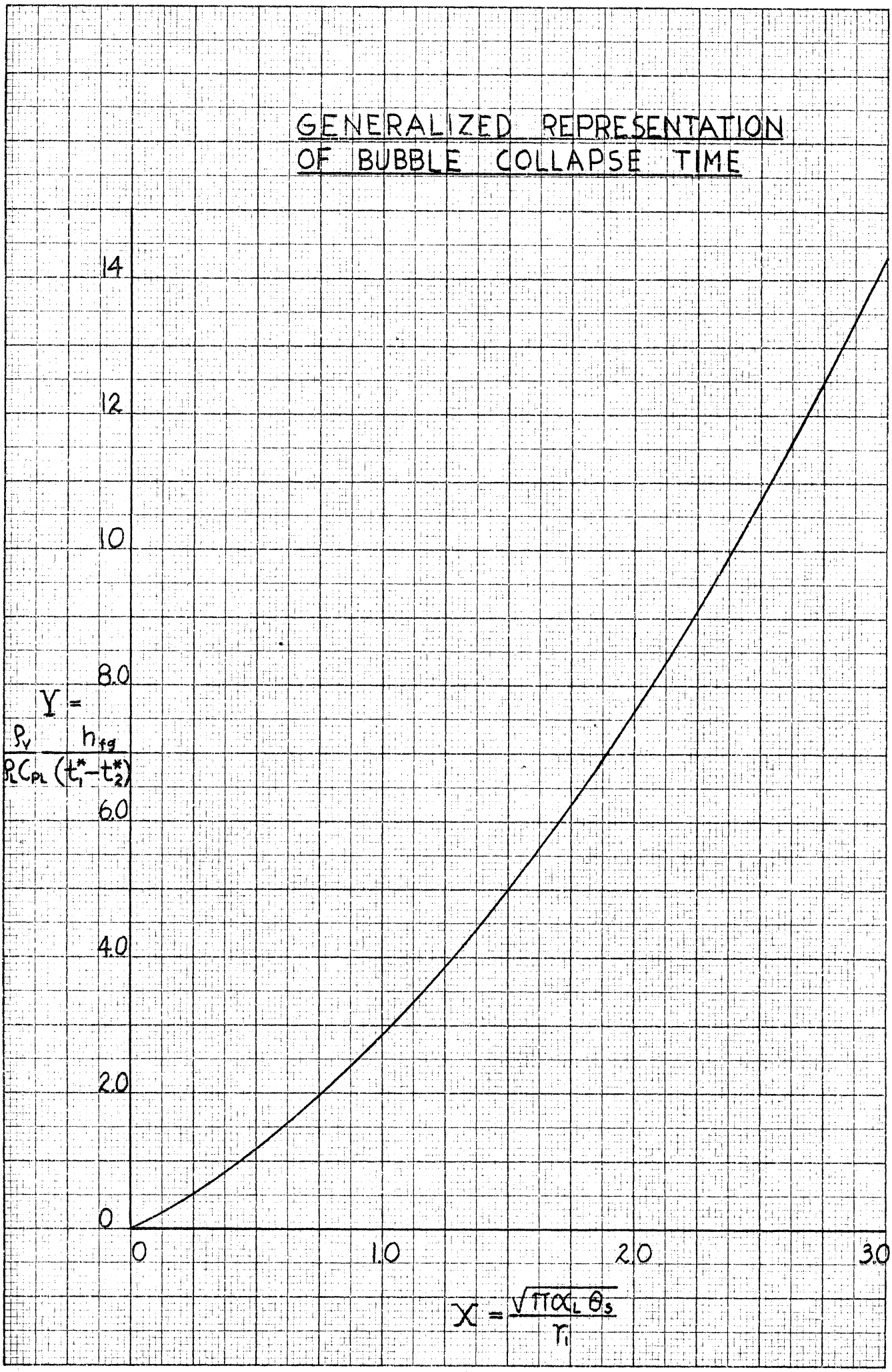
GENERALIZED REPRESENTATION
OF BUBBLE COLLAPSE TIME
14
12
10
8.0
6.0
4.0
2.0
0
Y = ρv hfg / ρL CpL (t1* − t2*)
0
1.0
2.0
3.0
X = √(π αL θs) / r1

FIG. 4

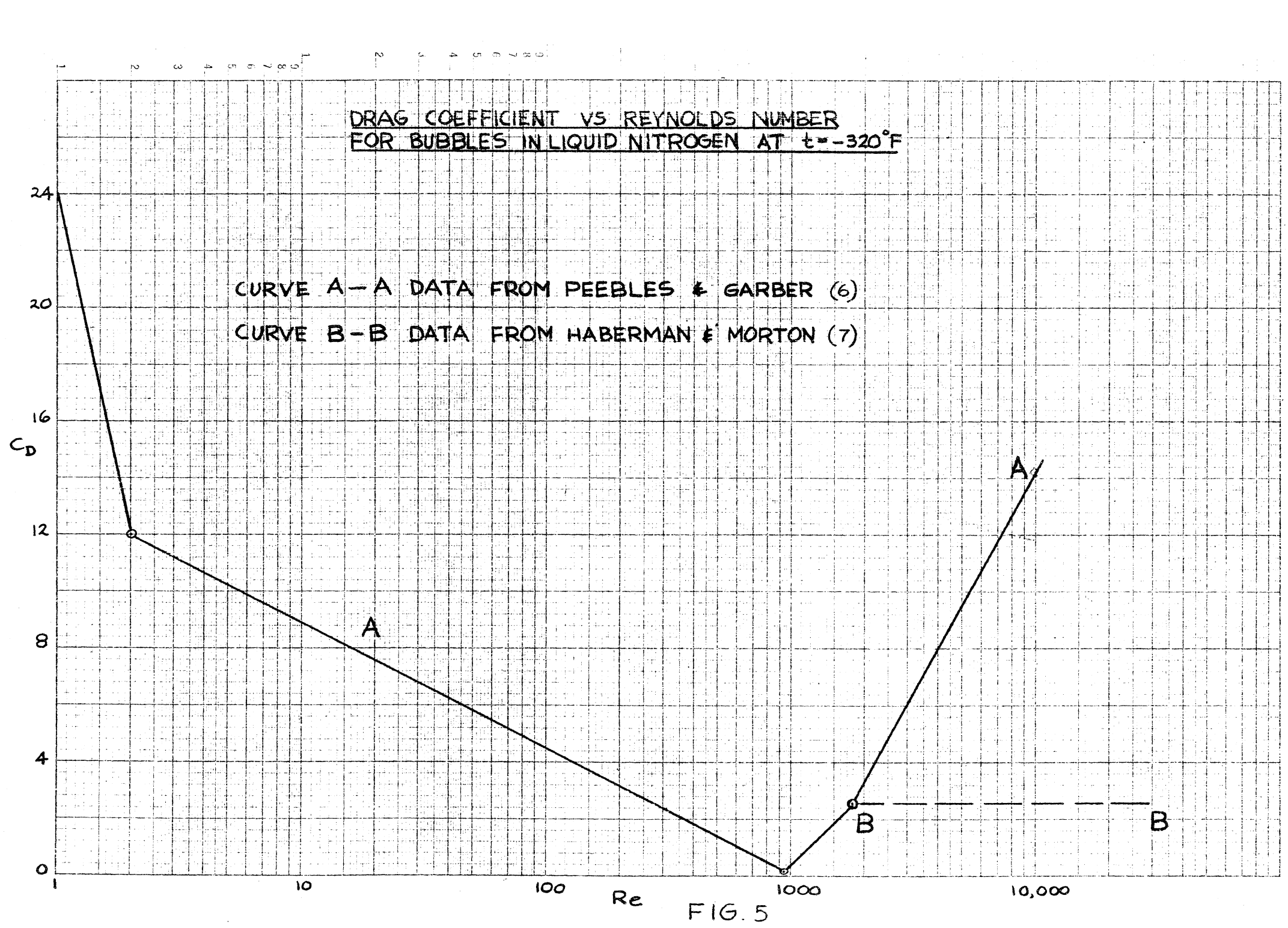
DRAG COEFFICIENT VS REYNOLDS NUMBER
FOR BUBBLES IN LIQUID NITROGEN AT t = -320°F
CURVE A-A DATA FROM PEEBLES & GARBER (6)
CURVE B-B DATA FROM HABERMAN & MORTON (7)
24
20
16
12
8
4
0
C_D
1
10
100
1000
10,000
Re
A
A
B
B

FIG. 5

TERMINAL VELOCITY OF NITROGEN VAPOR BUBBLES IN LIQUID NITROGEN

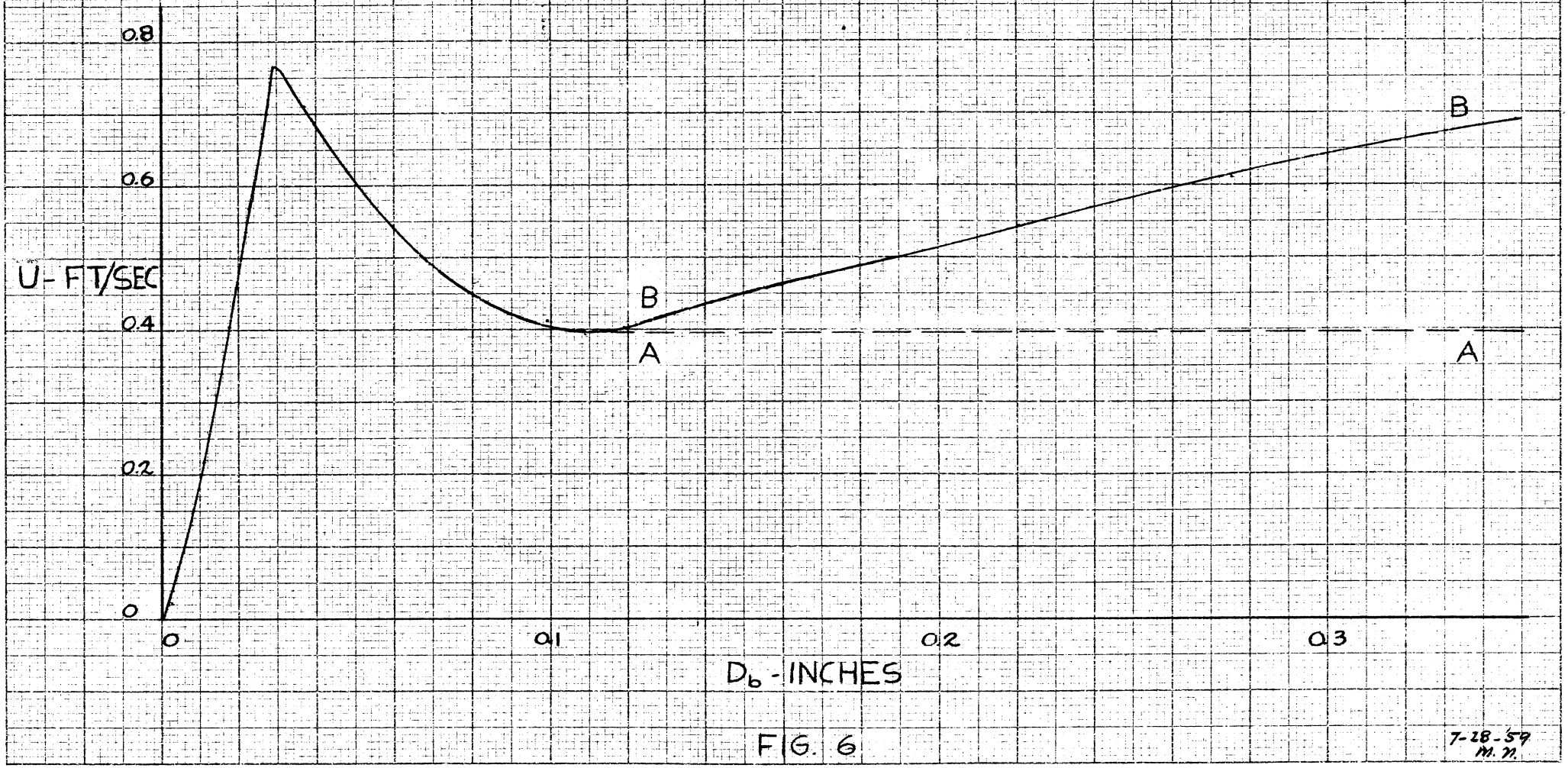

FIG. 6

7-28-59
M. M.

TERMINAL VELOCITY OF OXYGEN VAPOR BUBBLES IN LIQUID OXYGEN

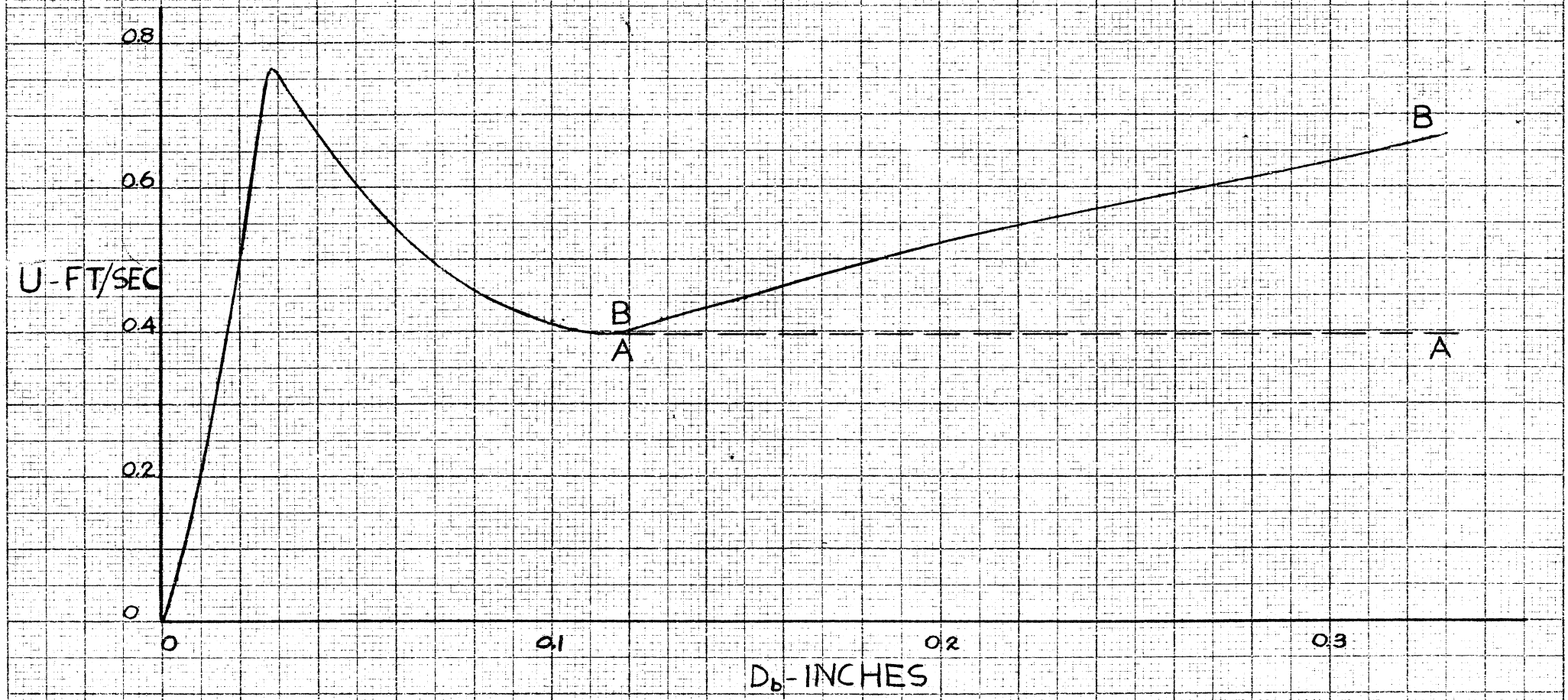

FIG. 7

7-28-59
M.N.

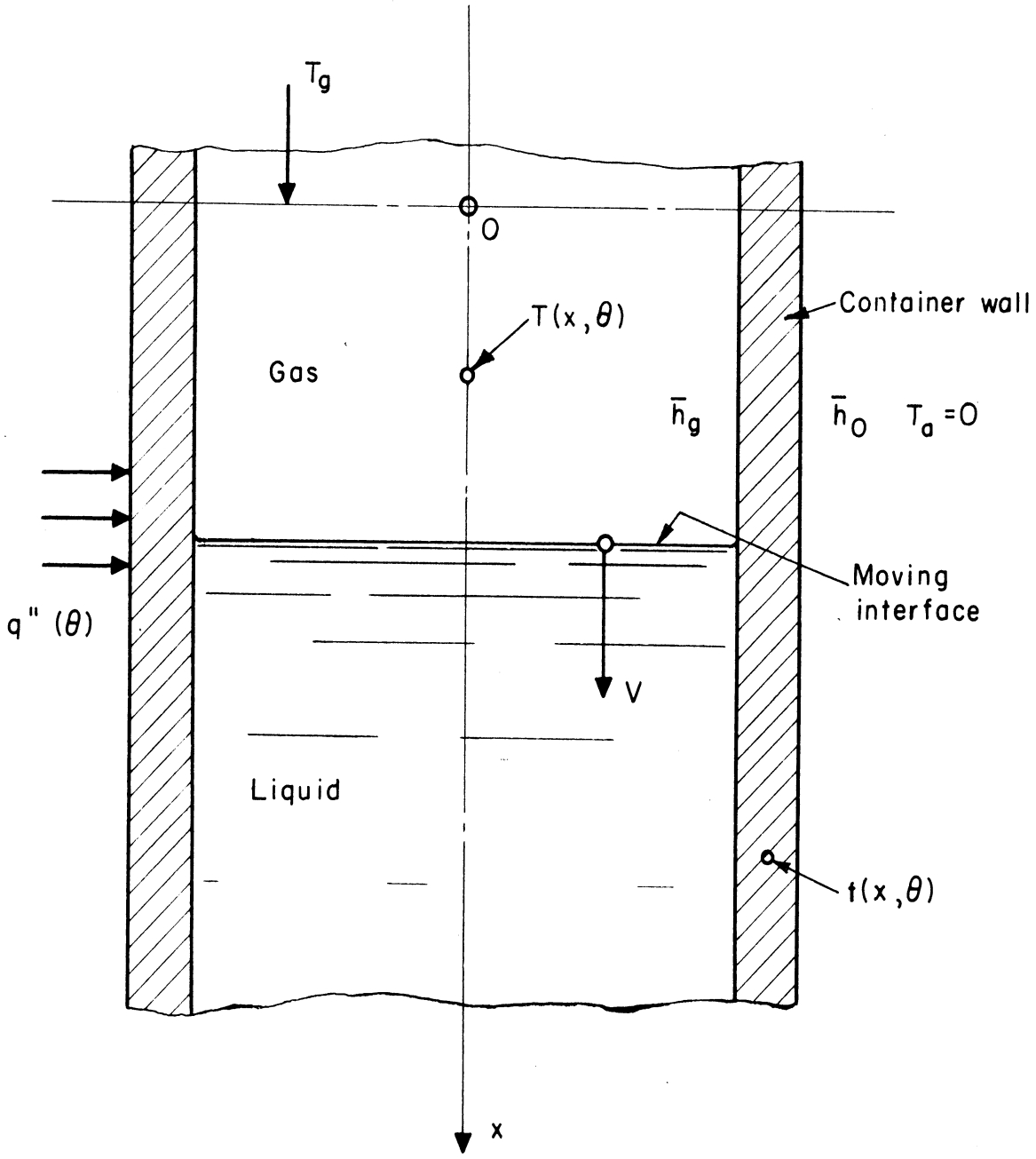
T_g
O
$T(x,\theta)$
Container wall
Gas
$\bar{h}_g$
$\bar{h}_O$ $T_a=0$
Moving interface
$q''(\theta)$
V
Liquid
$t(x,\theta)$
x

Fig. 8

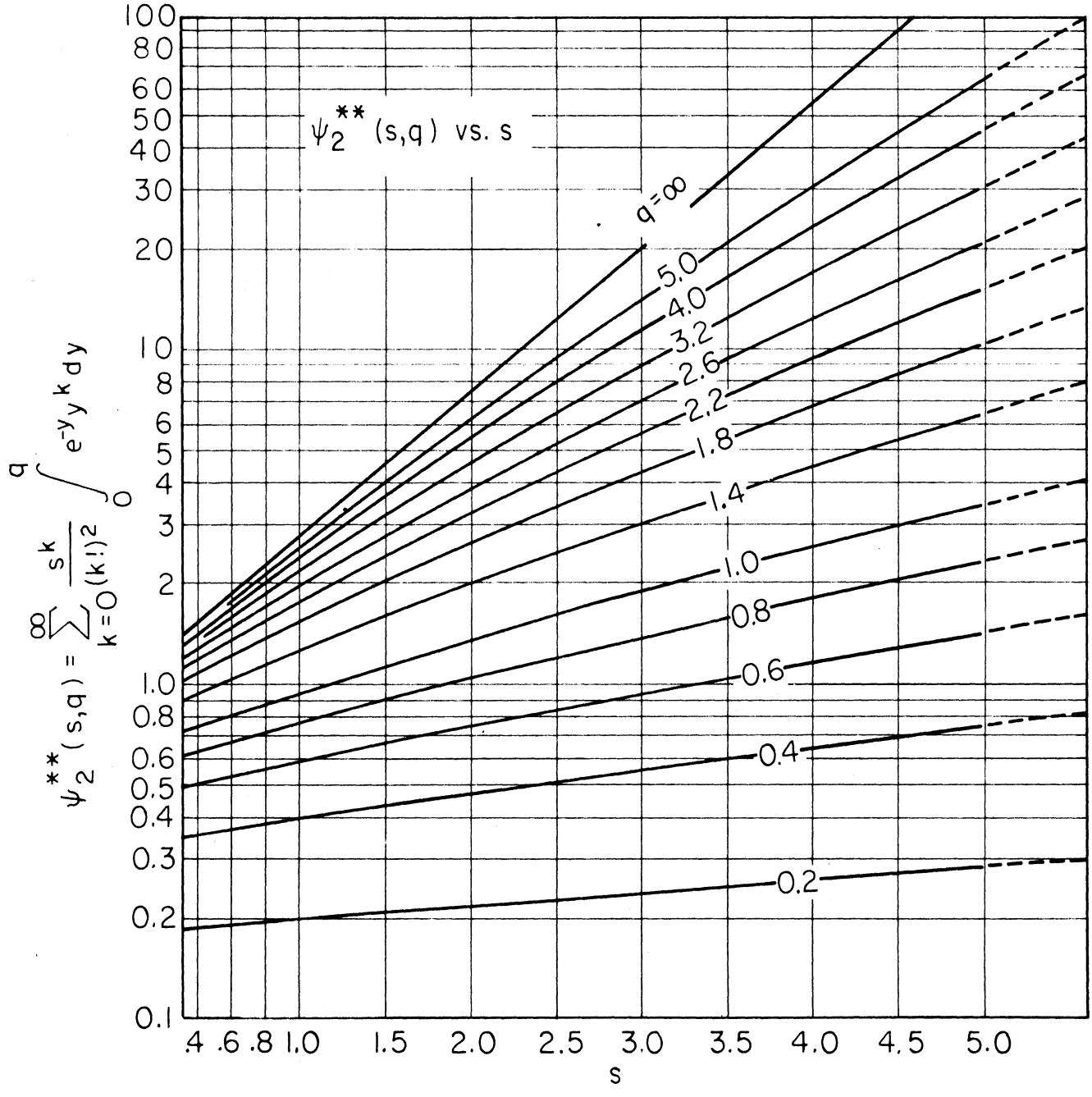

Figure 9

Note: See page 14 for explanation of nomenclature.